4,4'-dithiodipyridine on Au(111): a Combined STM, STS, and DFT Study

Berndt Koslowski, Anna Tschetschetkin, Norbert Maurer, and Paul Ziemann

Jan Kučera and Axel Groß

[1] Institut für Festkörperphysik, [2] Institut für theoretische Chemie, Universität Ulm, Albert-Einstein-Allee 11, D-89069 Ulm, Germany

We studied the adsorption of 4,4'-dithiodipyridine (PySSPy) on Au(111) under ultra-high vacuum conditions and at low-temperature both experimentally by means of scanning tunneling microscopy and spectroscopy (STM and STS), and theoretically by density functional theory (DFT). We find PySSPy molecules – characterized by their elongated appearance in STM – assembled in islands which reside exclusively in fcc regions of the herringbone reconstructed Au (HB) terraces. A triangular structure motif dominates the local arrangement of the PySSPy. DFT calculations reveal a virtually planar adsorption geometry of the PySSPy with the S-S bond of the molecule almost parallel to the Au-Au bonds of the substrate underneath. Though van der Waals forces dominate the stability of the adsorbed PySSPy, there is also a covalent contribution to the PySSPy/Au interaction. As a consequence, the PySSPy structures are relatively unstable. As found by STS, the highest occupied molecular orbital (HOMO) is located at around -0.7 eV below the Fermi energy (E_f) in good agreement with the HOMO provided by DFT. The position of the lowest unoccupied molecular orbital (LUMO) is about 3.2 eV above E_f leaving the HOMO-LUMO gap practically unchanged compared to a free molecule. The molecules exhibit a strong propensity to dissociate into monomers forming pyridine thiolates (PyS) at step edges or elbow sites of the HB. At room temperature, all PySSPy on the substrate dissociate resulting in linear chains of PyS characterized by a drop of the LUMO by about -0.9 eV.

Keywords: dithiodipyridine, scanning tunneling microscopy, scanning tunneling spectroscopy, density functional theory, van der Waal interaction, adsorption geometry

Introduction

Ever since the preparation of the first self-assembled monolayer (SAM) of organic molecules on top of an inorganic substrate, the field of organic-inorganic hybrid systems has rapidly developed both experimentally and theoretically. Presently, it is mainly driven by the highly requested advent of molecular electronics.[1] However, the host of properties achievable by combining the huge variety of organic materials with inorganic counterparts offers a plethora of applications beyond electronics. Corresponding examples are surface passivation,[2,3,4] corrosion protection,[5,6,7] wetting or de-wetting behavior,[8,9] lubrication,[10,11,12] catalysis,[13,14] and organic semiconductors[15] for, e.g., organic solar cells or organic light-emitting diodes.

Thiolates adsorbed on a gold substrate constitute the mostly investigated system due to the high affinity of sulphur to gold making stable surface modification feasible. SAMs of functionalized aromatic thiolates[16] covering a metal substrate have been studied intensively. It has furthermore been shown that such SAMs can be covered by a metal electrode. Such metal-molecule-metal junctions are considered to be building blocks of future molecular nano-devices.[17] Though a practicable procedure towards robust metal/SAM/metal junctions is not at disposal, yet, rather promising results have been achieved with a monolayer of Pd, Pt, and Rh on a SAM of 4-mercaptopyridine (MPy), 4-aminothiophenol (ATP), thiazole, or 1,4-dicyanobenzene anchored on a Au(111) substrate,[18] where the nitrogen atoms in the MPy molecule provide bonding to the top metal electrode. Recently, an entirely current-less process has been developed as an alternative to the previous electrochemical metallization.[19,20]

Preceding to the attachment of a top electrode, uniform SAMs on Au(111) are usually prepared from either organic or aqueous solutions of the specific molecules or their precursors. Though such SAMs are typically well organized and durable, the methodology suffers from two drawbacks: (i) contaminants in the solution may unintentionally be incorporated in the molecular junction deteriorating the intended function and (ii) a practical control over the arrangement of the molecules in the SAM and their localization on the substrate is not straightforward.[21,22] As an alternative strategy of SAM formation, one may employ sublimation of the SAM molecules onto the substrate under ultra-high vacuum conditions. This avoids contamination to a great extend, and it opens possibilities to control the SAM formation. Especially when using precursors, the prolonged pathway from deposition to the final SAM provides such possibilities. In the case of MPy, the

adsorption of which we studied earlier theoretically[41] and experimentally,[23,47] one uses typically 4,4'-dithiodipyridine (PySSPy) as a precursor to form a SAM from solution. Upon dissociation of the S-S bond at the surface and formation of two thiolates, the strongly binding MPy may self-organize at the surface.[24,25,26,27,28]

The theoretical description of the molecule/metal bonds represents still a rather challenging task for DFT because covalent bonds as well as the weak van der Waals (vdW) interaction and electron transfer effects are involved.[29] Commonly used exchange-correlation functionals neglect the dispersion forces and, hence, the description of the weakly interacting PySSPy by first principles is challenging. For a realistic description, DFT has to be corrected. In this study, we adopted two semi-empirical dispersion correction schemes, DFT-D3 [30] and DFT+vdW,[31] which have been used recently to model molecule/metal systems.[29,32,33] The methodology is based on supplementing the missing dispersion energy by a sum of pairwise interaction potentials expressed as a damped multipole expansion. This represents a rather effective tool, since, once the potential is known, there is basically no additional computational cost with respect to conventional DFT. Moreover, despite the fact that within the correction procedures the wavefunctions of the system remain unchanged, they allow to incorporate a specific chemical environment around each ion by (i) the evaluation of the pairwise potential from a Hirshfeld charge analysis within DFT+vdW and (ii) the interpolation between datasets of predetermined ab-initio polarizabilities in DFT-D3.

In order to elucidate the nature of the PySSPy/Au system experimentally and theoretically, we combined low-temperature scanning tunneling microscopy (LT-STM) together with density functional theory (DFT) calculations. The STM provides topographic information about the molecular structures on Au(111) and scanning tunneling spectroscopy (STS) delivers spectroscopic information about the electronic structure close to the Fermi level. We describe the system from pristine until PySSPy dissociated completely by annealing at room temperature without analyzing the dissociation process itself. DFT is employed to analyze especially the adsorption geometry and the electronic structures of a single PySSPy molecule at Au(111) as well as the basic structure motif formed by three PySSPy molecules as found experimentally.

Experimental

Commercial gold films on glass have been flame-annealed in a butane flame to develop extended {111} facets. After introduction into ultra-high vacuum (UHV), the films were exposed to a mild Oxygen plasma and annealed at temperatures up to 700° C to remove contaminants from the surface. We checked the gold surface by low-temperature STM ($p < 1\times10^{-10}$ mbar, $T \cong 5.5$ K)[34] ensuring that the {111} terraces were separated by straight monatomic steps and showed the well known herringbone reconstruction (HBR) of Au(111). Presumably due to strain in the annealed but still polycrystalline gold film, the HBR is not always exactly a $22\times\sqrt{3}$ reconstruction but the length of the mesh ranges from 20 to 22 with a period of ~(5.7-6.3) nm instead of 6.3 nm. Occasionally, we find small precipitates located at step edges. After checking the surface the samples were quickly transferred to the preparation chamber, and, from a home-built crucible, deposited 0.1 to 0.8 monolayers (ML) of 4,4'-dithiodipyridine (PySSPy; Aldrich) onto the gold film at a deposition rate of about 0.06 ML per second. After deposition, the samples were immediately transferred back to the low-temperature STM such that the sample returned to the STM after about 5 minutes. From the cooling behavior of the sample we conclude that the substrate temperature, T_s, was well below room temperature during deposition of the molecules and until it returned to the STM. A rough estimate from the cooling curve gives $T_s < -40$ °C at all times during deposition and transfer. The tunneling tips were electrochemically etched from a W wire, annealed at ~2000 °C in UHV, and conditioned by field emission and desorption at ~1 μA and < 1000 V.

Computational details

Self-consistent periodic DFT calculations were performed by means of the Vienna ab initio (VASP)[35] and Fritz Haber Institute ab initio molecular (FHI-AIMS)[36] simulation packages. In all calculations we applied the Perdew-Burke-Ernzerhof (PBE)[37] functional within the generalized gradient approximation (GGA) in order to describe exchange-correlation effects.

VASP calculation: The ionic cores were represented by projector-augmented wave potentials (PAW)[38] as designed by Kresse and Joubert.[39] The Kohn-Sham one-electron wavefunctions were expanded in a basis of plane waves with a cutoff energy of 400 eV. To include dispersion interactions, the DFT-D3 semi-empirical correction schema was adopted as constructed by Grimme *et al*..[30]

FHI-AIMS: A set of numeric atom-centered basis functions (NAO) were used to expand one-particle wavefunctions. The quality of the basis set was set 'tight' as a built-in option within the code. Scalar relativistic effects were included through the atomic-zora method. The dispersion interactions were described by the semi-empirical DFT+vdW method designed by Tkatchenko and Scheffler.[31]

In all calculations the Au substrate was represented by slabs of three-layers in which the top most layer relaxed during the geometry optimization while the other two Au layers were kept frozen at the positions corresponding to the Au bulk crystal optimized at the same level of theory. Note, that only Au atoms of the first layer were included in the dispersion correction to approximate a screening effect. In addition, the Au-Au dispersion interaction was deliberately excluded from the evaluation. Within the supercell approach the Au slabs were separated by a vacuum gap of thickness 2.2 nm.

Super-cells comprising 5x5, 6x6, and 8x8 unit cells of the Au(111) surface were used to model a single PySSPy molecule as well as the clusters of three PySSPy. In order to perform the integration across the Brillouin zone, a Monkhorst-Pack grid of 5x5x1, 3x3x1, and 1x1x1 *k* points were used, respectively. During geometry optimization, the structures were allowed to relax until the total energy changed less than $1x10^{-5}$ eV and the residual forces changed less than 0.01 eV/Å. The STM images were simulated according to the Tersoff-Hamann approach[40] to allow for a direct comparison with the experimental STM images.

Results and discussion

After deposition of PySSPy molecules corresponding to ~0.3 monolayers (ML) on the cold gold surface, two different objects representing molecular structures can be recognized in the topographical images (see Fig 1(a) and (b)): (i) small spherical objects (marked as O1) located mostly along step edges between terraces or at elbow sites of the HBR (see Fig. 1(a)), and (ii) oblong objects (labeled as O2) located predominantly in larger clusters within fcc regions of the HBR (see Fig. 1(b)). Interestingly enough, in the case of O2 objects adjacent to a terrace step edge, there are always O1 objects sitting directly at the step edge and so separating the O2 assemblies from the step edge (see lower left corner of Fig. 1(a)).

The O1 objects are interpreted as MPy molecules adsorbed at the gold surface. It appears that these molecules occupy preferentially defect sites, i.e. step edges and elbow

sites, which are the most active sites at the Au(111). The observation of MPy monomers demands for PySSPy dissociation and a subsequent formation of MPy/Au complexes.[41] We include here the experimental description of the dissociation to draw a broader picture of the investigated system. The discussion of the dissociation, however, is a topic on its own and shall be postponed to a later contribution.

The O2 objects are assigned to non-dissociated PySSPy molecules occupying planar fcc regions of the (111) surface. PySSPy are almost exclusively arranged in clusters or islands. These arrangements of molecules modify the surface reconstruction of the gold by expelling hcp regions from island regions as obvious from the soliton walls girding the islands (see Fig 1a). Within the islands of PySSPy (O2 objects), one finds a relatively high degree of disorder. One reason for that disorder is MPy molecules (O1 objects) scattered all over the surface. The most probable reason for that disorder might be mutual steric restraints at the lowered deposition temperature leading to metastable lateral arrangements of PySSPy molecules, while increasing the temperature results practically in their complete dissociation. Most PySSPy molecules form groups of three molecules in a triangular arrangement and rotated mutually by 60°, in other words, they compose a triskelion. This basic triangle can be most frequently found in our STM images, e.g., close to step edges and within islands together with its mirrored counterpart. In most islands the basic triangle is surrounded by additional molecules being almost parallel to each of its sides thus forming a doubly walled triangle (cfg. 1(b) and 3(c)). The outer PySSPy enclose an angle of ~15° with the inner PySSPy.

Such a doubly walled triangle can be seen at the basis of the island structure shown in Fig. 1(b) where one outer molecule is missing at the lower right side. The extrapolated unit mesh in the island would be about $15\times3\sqrt{3}$ (compare Fig. 3(d)) since the triangle in the center of the mesh has opposite chirality. Consequently, the number of left and right handed triangles and molecules is equal in this structure.

To unveil the microstructure of the PySSPy/Au(111) we carried out a modeling of the PySSPy adsorption on the defect-free Au(111) surface using DFT-D3. Three tasks were addressed: (i) find the most stable adsorption structure of isolated PySSPy on Au(111), (ii) elucidate the nature of the PySSPy/Au contact, and (iii) make a connection between the triangular arrangement observed in STM images and the corresponding triangular configuration of PySSPy molecules on Au(111). The results will be described in the following.

In the gas phase structure depicted in Fig. 2(a), the PySSPy molecule has a boat-like conformation with a dihedral angle of the C-S-S-C bond of about 84°. To achieve the most stable structure on Au(111), the molecule unfolds substantially and adopts a virtually planar arrangement in which the molecule is almost parallel to the gold surface and the two sulfur atoms are somewhat closer to the surface above two neighboring Au atoms. The optimized geometry of a PySSPy on Au(111) within a 5×5 unit cell is shown in Fig 2(b) (side view) and (c) (top view). The length of the S-Au bonds is 2.83 Å and 2.84 Å. The C-S-S-C dihedral angle increases, with respect to the gas phase structure, to 156°, and the separation of a nitrogen atom in the PySSPy molecule from the nearest Au atom is ~3.5 Å. The top view (see Fig. 2(c)) reveals that the S-S bond is almost aligned with the Au-Au bond underneath. Projected onto the surface plane, the S-S and Au-Au axes, i.e., <10$\bar{1}$>, enclose an angle of only 7.3° and the structure is point symmetric about the center of the Au-Au or S-S bonds. The projected N-N axes point approximately in <51$\bar{5}$> enclosing an angle of ~70° with the Au-Au reference axes. This is again ~10° with respect to a <10$\bar{1}$> direction.

The energy gain upon adsorption of a single PySSPy molecule, E_{ads}, is about -1.37 eV where E_{ads} was calculated according to E_{ads}= E(PySSPy/Au) – [E(PySSPy) + E(Au)] with the optimized total energy of a PySSPy on Au(111) within a 5x5 surface unit cell, E(PySSPy/Au), the total energy of a single gas phase molecule calculated within a 8x8 surface unit cell, E(PySSPy), and the bare Au(111) substrate relaxed within a 5×5 unit cell. On one hand, opening the C-S-S-C dihedral angle of the molecule costs ~0.36 eV of deformation energy per molecule. On the other hand, the flat configuration saves ~1.61 eV arising from inter and intra-molecular dispersion interaction given by the semi-empirical pair-wise contributions. Despite of this large dispersion interaction, the approximate alignment of the S-S bonds with Au-Au bonds as observed in STM images suggests that there is a significant contribution by covalent bonding. To show this we calculated the electronic structure of the molecule/metal interface with the total density of states (DOS) and the local DOS (LDOS) projected onto particular ions. The graph of the DOS along with the LDOS projected onto the atoms in the molecule and the Au atoms of the 1st layer are shown in Fig. 2(e). In the region of the valence band, hybridization of molecular and gold states is visible from the minor and major peaks at about -0.6 eV (highest occupied molecular orbital, HOMO) and -1.1 eV (HOMO-1), respectively. To further support the picture of interacting molecular and metal wavefunctions, we constructed a charge-density difference plot depicted in Fig. 2(f). There, the charge accumulation in the region between

the S and the Au atoms shows the partial covalent bond character though the S-Au bonds are relatively long.

Recapitulating the theoretical findings so far, the dispersion interaction drives the molecule against an increasing deformation energy into the flat lying configuration and partial covalent bonds between the S and Au atoms register the flat molecule with the substrate such that the S-S of the molecule is approximately above the Au-Au of the substrate. Finally, we checked whether the structure optimized within a 5x5 unit cell would change with increasing cell size due to a decreasing intermolecular interaction with molecules of neighboring cells. Calculations employing a 6x6 and 8x8 unit cell resulted in equivalent geometries and showed that the 5x5 model is a valid model of an isolated PySSPy molecule on Au(111).

As inferred above, inclusion of dispersion forces is indispensable in order to describe the molecule/metal complex correctly. To analyze the performance of DFT-D3 in comparison to a different DFT+D correction scheme, we carried out a DFT+vdW optimization of corresponding PySSPy/Au models within a 5x5 unit cell of the Au(111). After optimization we obtained very similar planar configuration of PySSPy on Au(111) in a perfect agreement with DFT-D3. DFT+vdW resulted in a slight prolongation of the S-Au bond by ~0.08 Å with respect to DFT-D3. Surprisingly, the adsorption energy, E_{ads}, is significantly greater in DFT+vdW (-1.86 eV) while the contribution of the dispersion interaction is smaller (-1.37 eV). The latter arises mainly from the molecule/Au interaction. Our findings confirm results of earlier studies[29,33] that there is some scatter among different semi-empirical dispersion correction schemes. The large discrepancy in E_{ads} between both methods could be ascribed to a different balancing of the interaction of the Au substrate with the S atoms and the aromatic rings of PySSPy. Yet, both methods agree in that PySSPy is bonded to Au(111) in a flat geometry.

In order to compare the optimized theoretical arrangement of the PySSPy with STM images, we adopted the Tersoff-Hamann approach to simulate an STM image. The theoretical STM image of a single PySSPy on Au(111) is depicted in Fig. 2(d). It shows an oblong entity aligned with the N-N direction of the adsorbed molecule in agreement with the cigar-like motifs revealed by experimental STM. Based on the calculations, the angle between the longitudinal axes of the O2 object and $<10\bar{1}>$ directions is ~70° in good agreement with experimental STM images.

In the last step, the arrangement of three molecules in the triangular structure which is the local structure motif in experimental STM images was examined theoretically. To accomplish that, we performed a full optimization of three PySSPy molecules on Au(111) within a 8x8 surface mesh. The result is shown in Fig. 3(a). Upon full optimization, each molecule takes a position almost identical to the planar arrangement of an isolated molecule on Au(111). The molecules are mutually rotated by 60º and all S-S bonds point along the Au-Au bonds underneath. The average length of S-Au bonds is 2.85 Å. The shortest separation of N···H between N···H-C contacts is 2.22 Å suggesting a rather weak H bond. Assembling the three originally isolated PySSPy molecules on Au(111) in the triskelion causes an energy gain of only 0.10 eV per molecule which is 0.30 eV per complex. Interestingly, in a hypothetical triskelion in gas phase in which all molecules are frozen in its planar conformation, the optimized N···H distance is slightly longer (2.33 Å) due to a small repulsive intermolecular H-H interaction. Consequently, the separation of Au atoms in the {111} surface fits rather accidentally to the triskelion in gas phase and registering with the substrate is governed by the S-Au bonds of each molecule. Finally, we simulated the STM image of that optimized 3PySSPy/Au complex (Fig. 3(b)). The calculated image resembles very much the basic triskelion occurring in experimental STM images. Figures 3(c) sketches a possible layout of PySSPy molecules in the doubly walled triskelion. This triskelion consists of 6 molecules: the three PySSPy molecules of the inner triangle have identical chirality, however, the three outer PySSPy have opposite chirality. From a simple symmetry argument, the enantiomer exists and, hence, the whole structure is chirality-neutral. Figures 3(d) sketches the possible layout of the basis from which the islands in Fig 1(d) are built. There, the lower outer PySSPy of the doubly walled triskelion is missing, and this broken triskelion is supplemented by its mirrored counterpart at the upper right side. Also this structure is chirality-neutral.

Summarizing our theoretical considerations, we find the agreement of theory and experiment very convincing. This signifies that DFT-D3 and DFT+vdW can be applied reliably to a molecule/metal interface while non-corrected DFT is definitely not sufficient.

In order to learn experimentally more about the electronic structure of the molecules, we gave *z*-*V* spectroscopy precedence over *I*-*V* spectroscopy. Here, the topographic feedback-loop of the STM is left on while scanning the sample bias, *V*, and acquiring the tip-sample separation, *z*, together with the conductivity, $\partial_V I$, i.e., at constant tunneling current, *I*. $\partial_V I$ is still a measure of the change of tunneling probability with sample bias and,

therefore, a measure of the LDOS.[42,43] This spectroscopy mode leads to a gentler treatment of the sample since an increasing tunneling bias causes an increasing tip-sample separation. To refine the method a bit, we multiply $\partial I/\partial V$ by V to obtain a better measure of the LDOS, ρ. We understand this easily by writing the tunneling current as $I = I_0 \frac{V}{V_0} T(z)$ for an arbitrary state compared with a reference state indicated by the subscript Null. Φ is the apparent tunneling barrier height at zero bias, and the transmission probability function is $T(z) = e^{-\sqrt{\Phi}z}$. Prerequisite of the given equation is a constant LDOS. For two states having the same current we obtain $\left(\mathrm{z} = \frac{1}{\sqrt{\Phi}} \ln\left(\frac{V}{V_0}\right) + z_0\right)_{\mathrm{I_0}}$ and, hence, the transmission factor is approximately $\left(T(z) = \frac{V_0}{V} e^{-\sqrt{\Phi} z_0}\right)_{I_0}$. With $\rho \approx \frac{1}{T}\frac{\partial I}{\partial V}$ [37,43,44] we arrive at $\left(\rho \approx \frac{V}{V_0 e^{-\sqrt{\Phi} z_0}} \frac{\partial I}{\partial V}\right)_{I_0}$ showing the desired relation $\left(\rho \sim V \times \frac{\partial I}{\partial V}\right)_{I_0}$ as a rough but, here, sufficiently accurate estimate.

Fig. 4 shows separate *z-V* measurements for the two signs of the sample bias measured on the bare Au(111) close to a molecule (red curves) and on a molecule in an island. For gold, we find a sharp increase at +3.8 eV indicative of the upper edge of the *L* gap in gold. On PySSPy, however, we find a pronounced peak at about 3.2 eV which we attribute to the lowest unoccupied molecular orbital (LUMO) of PySSPy. These peaks can be nicely fit by a Lorentz curve (not shown) with a width of ~0.8 eV corresponding to a lifetime of the electrons in the LUMO of ~0.8 fs. The position and the width of the LUMO depend slightly on the coordination of the molecules: in a corner at the boundary of an island (lowest coordination) the position/lifetime is +(3.36±0.014) eV/0.70 fs (Fig. 4(b), green curve), at the boundary +(3.22±0.033) eV/0.70 fs (Fig. 3(b), marine curve), and within the island +(3.16±0.022) eV/0.85 fs (Fig. 4(b), magenta curve), respectively: the position of the LUMO shifts to lower values for higher coordination while the lifetime increases. Assuming a lifetime, τ, limited by electron-electron interaction with an inverse square law $\tau = \tau_1/E^2$ as for bulk electrons (with E in eV), τ_1 would be (8.15±0.19) fs similar to transition metals. So it appears to us that the lifetime of electrons in the LUMO of the molecule is limited by a similar mechanism as for electrons in the ground state of the Shockley-like surface state.[45] There, the life time of electrons in the surface state is mainly determined by interaction with electrons in the bulk kicking the electron on and off the surface state.

For occupied states (negative sample bias) the situation is less satisfactory. This is always the case in STS since electrons in occupied states experience a higher tunneling barrier than those in unoccupied states.[46] Differences in *z*-*V* curves for bare Au(111) and PySSPy are small but exceed significantly the limit of experimental accuracy (~1%). The most significant difference is an increased LDOS on PySSPy at around -0.8 eV within the surface gap between the onset of the Shockley-like surface band (-0.47 eV) and the lower edge of the *L* gap (-1.1 eV). Setting the highest occupied molecular orbital (HOMO) to this value, which is in great correspondence with the theoretical DOS, the optical gap of the PySSPy would be about 4.0 eV, close to the expected value for a free PySSPy molecule. In addition, the LDOS of the molecule appears to be enhanced around -1.4 eV and around -2.0 eV at the upper edge of the *d* bands of gold. Note that if we compare the result for PySSPy in the negative energy range to that obtained for MPy/Au(111),[47] PySSPy behaves very similar to MPy molecules aligned in a linear chain. As far as the comparison between calculated (Fig. 2(e)) and measured (Fig. 4) LUMO is concerned, the typical band-gap problem of DFT is obvious: the calculated LUMO is at lower energy than the measured one. Still, the widths compare favorably. Thus, the DFT calculations confirm the coupling between the unoccupied states of the molecules and the substrate.

In Figure 5 we present the apparent molecular height of PySSPy in dependence of the tunneling bias. As in the case of MPy[47] and terthiophene (3T) on Au(111),[48] the bias dependence segments into 3 regions. For a bias $V_t < 0$ eV, the molecular height, h, depends marginally on bias. For 0 eV < V_t < 1.5 eV, h is almost independent of the bias at approximately $h \cong 0.15$ nm, and, for $V_t > 1.5$ eV, h increases linearly at a rate of approximately $\partial h/\partial V_t\big|_{It} \cong 0.1$ nm/eV resulting in an extrapolated height of the molecule of ~0.32 nm at the bias corresponding to the LUMO (+3.2 eV). Consequently, our interpretation of STM/STS on PySSPy is similar as in the cases of MPy and 3T: Occupied states of the sample contribute little to the tunneling current and, hence, the HOMO is spectroscopically and spatially poorly resolved. In the bias range 0 V < V_t < 1.5 eV, tunneling is dominated by unoccupied states of the sample belonging to a locally modified surface state of the Au(111). The modification consists primarily in bulging of the surface state outwards from the surface which amounts to the apparent molecular height measured in that bias range 0 < V_t < 1.5 eV (0.155 nm). The magnitude of bulging should be related to the polarizability of the molecule perpendicular to the surface. Above 1.5 eV the LUMO of the molecule contributes increasingly to the tunneling current and, hence, the tip withdraws from the surface. Since the surface state of Au(111) is approximately half a

Fermi wavelength (~0.15 nm) in front of the nuclear plane of surface atoms, the geometric height of the molecule would be (0.32+0.15) nm = 0.47 nm. Note that, this is slightly overestimating the separation of the nitrogen atom from the nuclear surface plane of the theoretical structure (0.34 nm). However, the measured molecular height is typically influenced by the tunneling barrier height decreasing with increasing bias.[46,47,48] This barrier effect entails an increased apparent molecular height. Unfortunately, we did not succeed in differential barrier measurements because the molecules underwent slight modifications during the measurements; i.e., the molecules were not stable enough under low bias, i.e., at low tunneling resistance and tip-sample separation.

The presented adsorption behavior of the PySSPy is not very stable under tunneling conditions even at a temperature of $T < 6$ K and a tunneling current $I_t \cong 50$ pA. If acquiring repeatedly *z*-*V* scans as shown in Figure 4(b) at an elevated tunneling current (>100 pA), we observe frequently a sudden and irreversible change of the measured *I*-*V* curves. The modification consists primarily of a shift of the LUMO down to +(2.5±0.15) eV and is accompanied by a slight change of topography. The sudden change occurred always at a bias close or above the energy of the LUMO. Since these modified curves are similar to curves measured on MPy aligned in linear chains (LUMO centered at 2.0 eV),[47] it is well conceivable that the PySSPy had dissociated due to electrons passing across the LUMO leaving a pair of proximate MPy/Au complexes. Such sensitivity to low-energy electrons has been observed for aliphatic disulfides by applying current pulses with an STM.[28]

Above, we demonstrated that the low-temperature UHV sublimation technique can be used to deposit molecular assemblies of non-dissociated PySSPy molecules on a planar gold substrate. In a further step, we accomplished complete dissociation of the PySSPy to form the MPy/Au complex in agreement with earlier studies.[24,25] To do this, we annealed the sample at room temperature for 5-10 minutes and then cooled it back to ~6 K. Figure 6 presents the experimental changes due to this annealing. The molecules now appear aligned in chains along the HBR (see Fig. 6(a)) similarly as MPy did after annealing at room temperature.[47] Note, that the chains shown here look much more disheveled than those shown in Ref. 47. Six-fold nodes give the molecular chains the opportunity to bridge over neighboring hcp regions to the next fcc region. Within the chains beads can be recognized. The beads have a length/period along the HB of ~0.75 nm and a width of ~0.8 nm. We assume that the beads are formed by pairs of thiolates. A topographic hint to that assumption is given by the open ends of chains in Figure 6(a). Many of these open

ends cease by a smaller entity which could be a mono-thiolate. Another hint is given by the electronic structure of the chains (Fig. 6(b)). While the occupied states in the chains are difficult to distinguish from single PySSPy or islands of those, the LUMO shifted down significantly to (2.1±0.1) eV in 50 % of cases. This is equivalent to MPy after annealing where the molecules formed linear chains and the LUMO shifted downwards by -1.2 eV to 2.0 eV.[47] In the other 50% of cases, the *z-V* measurement on the chains is not stable or shows double peaks at, e.g., 2.3 eV and 3.0 eV, as shown in Figure 6(b). Unfortunately, we did not obtain sufficient lateral resolution to resolve the structure of those beads.

Conclusion

We investigated the adsorption behavior of PySSPy on Au(111) at low temperature under vacuum conditions by means of a combination of scanning tunneling microscopy and theoretical modeling using density functional theory.

The topographic findings are that (i) the molecules form a large superstructure in fcc areas of the Au(111) terraces based on a triskelion comprising 3-6 molecules. Corroborated by DFT calculations, PySSPy adsorbs in a flat but sulphur-down geometry with two S-Au bonds. The S-S bond as well as the N-N axis of the molecule is then approximately aligned with atomic rows of the subjacent substrate. The degree of disorder in islands of PySSPy is relatively high presumably because of scattered mono-thiolates and a high degree of degeneracy in that large spatial structure. (ii) PySSPy dissociates presumably at step edges of the Au(111) and at the elbow sites of the herringbone reconstructed Au(111) surface resulting in single pyridine-thiolates. In STS we find the LUMO at +3.2 eV above the Fermi level and the HOMO hardly resolved at -0.7 eV below the Fermi level. At room temperature migration of the molecules is high enough to dissociate all adsorbed molecules within few minutes. Then, the molecules form linear chains of pyridine-thiolates. The degree of disorder, however, is relatively high as compared to the case of MPy which could be a significant difference in further processing the molecular layers.

Acknowledgements

We are indebted to the Deutsche Forschungsgemeinschaft for generous support by the collaborative research unit SFB569 TP C5 and A8. The free program 'ImageJ'[49] was used to display images in 3D representation. Computational resources have been provided by the bwGRiD[50] project of the Federal State of Baden-Württemberg/Germany.

Additional support by the Baden-Württemberg-Stiftung through project B1 of the Competence Network "Functional Nanostructures" is also gratefully acknowledged.

Figures and captions

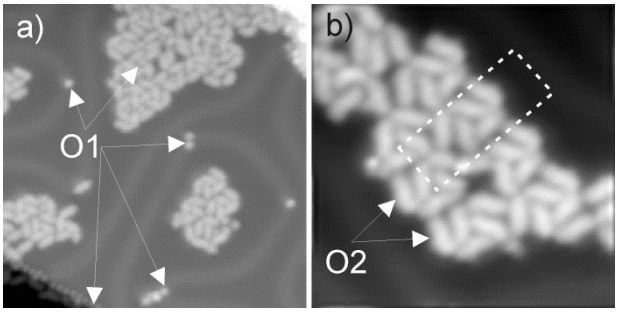

Figure 1: Topographic images of the Au(111) covered with PySSPy. (a) Top-view of a single terrace showing the most important features: (i) islands of PySSPy within fcc regions surrounded by the HBR, (ii) single molecules of PySSPy, (iii) single molecules of MPy (objects O1 as indicated by arrows), and (iv) MPy at the base of steps (14 nm × 14 nm × 0.54 nm; V_t = 1.1 eV, $I_t \cong$ 30pA). (b) Magnified top view onto an island showing a windmill structure (6 nm × 6 nm × 0.21 nm; V_t = 1.1 eV, $I_t \cong$ 30pA). The white rectangle indicates an extrapolated unit mesh. All figures are using the same color coding (gray scale).

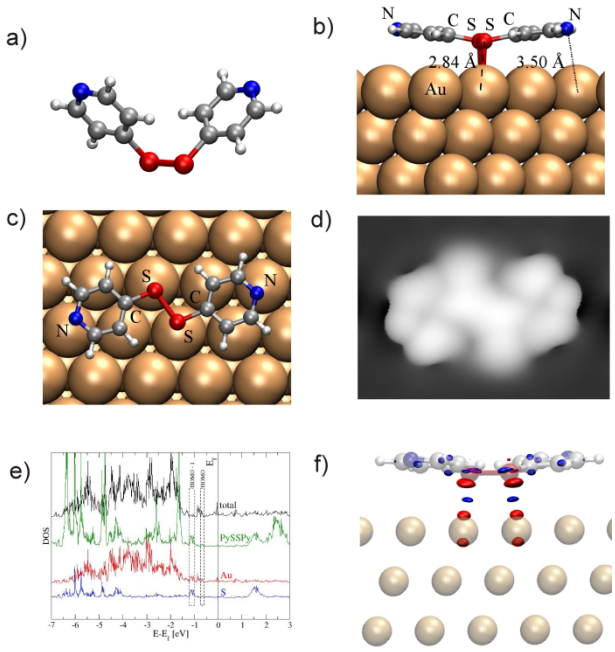

Figure 2: (a) Side view of the optimized geometry of a PySSPy molecule in the gas phase (colors: red – S, gray – C, white – H, blue – nitrogen). Side view (b) and top view (c) of the optimized geometry of a single PySSPy molecule adsorbed on Au(111) within a 5x5 unit cell. In top-view, the N···N axis is rotated by ~63° with respect to the S-S axis which is rotated by ~7° with respect to the atomic rows of Au. Panel d) represents the STM

topography of the PySSPy/Au(111) structure according to the Tersoff-Hamann approach. Size and orientation correspond to panel (c). (e) Density of states (DOS) calculated for PySSPy/Au(111) within the 5x5 periodic model. 1st (upper) curve: total DOS of the system (multiplied by a factor of 0.1). 2nd curve: local density of states (LDOS) summed up for all atoms of the PySSPy molecule. 3rd curve: LDOS summed up for the gold atoms in the first layer of the Au slab. 4th (lower) curve: LDOS of the sulphur atoms. (f) Plot of the charge density difference in a plane perpendicular to the surface. The blue and red areas wrap the regions of charge accumulation and depletion, respectively.

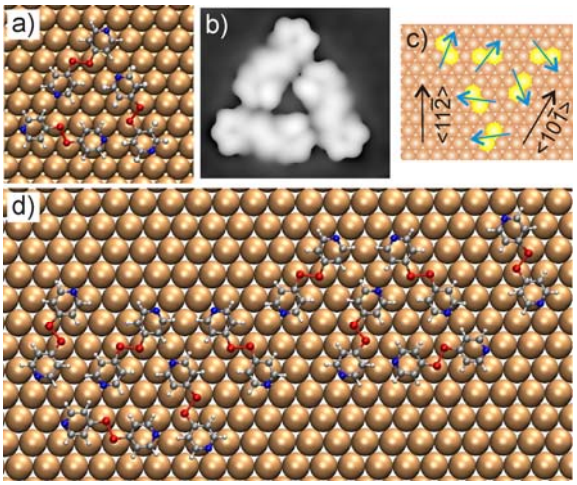

Figure 3 (color): (a). Top view of the optimized triangular arrangement of three PySSPy molecules on top of a planar Au(111) surface and (b) the simulated STM image of that structure according to Tersoff and Hamann. In top-view, The N···N axis is rotated by ~68° with respect to the S-S axis which is aligned with the atomic rows of the Au. Size and orientation of panel (b) corresponds to panel (a). (c) Schematic model of the absorption geometry with respect to the Au(111) surface. Yellow surface atoms are covered by the S-S axis of the molecule forming S-Au bonds. The blue arrows represent the orientation of the N-N axis (pointing approximately in <51$\bar{5}$> directions) and the length corresponds to the N-N separation. The resulting triskelion matches the triangle at the lower left corner of the rectangle in Fig. 1(b) where the lower outer molecule is missing. (d) Model of the basis of the unit mesh formed by the PySSPy molecules. The right windmill has opposite chirality as compared to the left one. The periodic repetition of the molecular arrangement would result approximately in an $18 \times 3\sqrt{3}$ unit mesh having very low symmetry (note: in the theoretical models one tends to form a larger mesh than found experimentally).

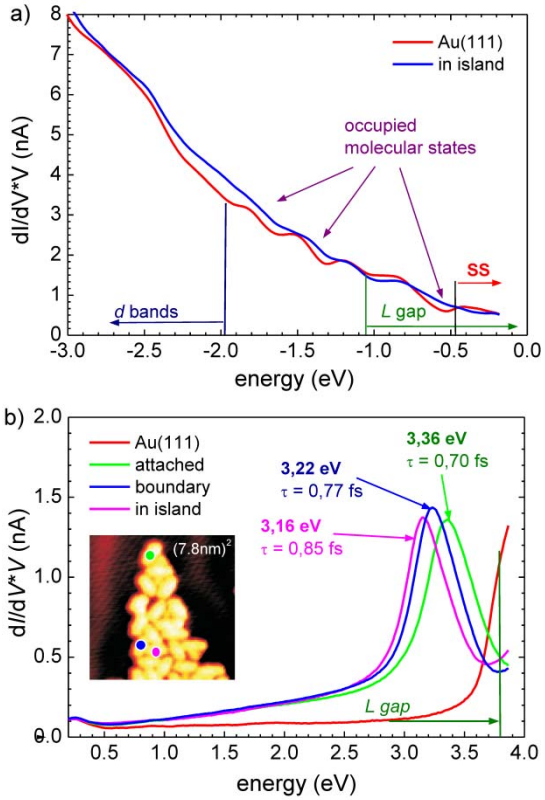

Figure 4 (color): *z-V* measurements for occupied (a) and unoccupied states (b) of a PySSPy molecule in an island. Shown are $V \times \partial_V I$-V curves as explained in the text. One easily recognizes the LUMO. The HOMO, however, is difficult to resolve. The inset in panel (b) indicates with corresponding colors the positions in an island where the *z-V* measurements have been performed.

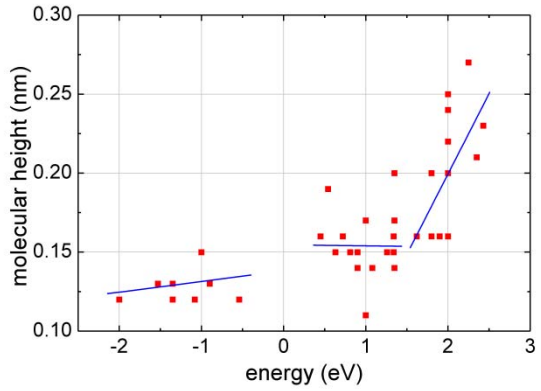

Figure 5 (color): Molecular height of PySSPy with respect to the Au(111) in dependence of the tunneling bias. Straight lines indicate piecewise linear fits to the data. The extrapolated height at the energy of the LUMO (3.2 eV) is about 0.32 nm. In particular,

the fits are for V_t < 0 eV: h = (138±13) pm + (6.8±9.9) pm/eV × V_t, for 0 eV < V_t < 1.5 eV: h = (155±16) pm + (-1±15) pm/eV × V_t, for V_t > 1.5 eV: h = (-4±66) pm + (-102±33) pm/eV × V_t.

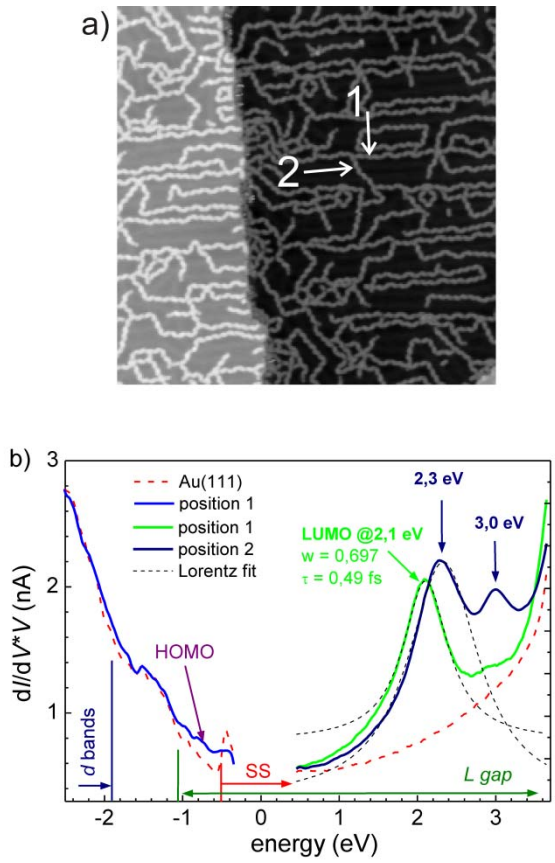

Figure 6 (color): PySSPy covered Au(111) (0.3 ML coverage) after annealing at RT for 5 minutes. (a) Topography (40 nm × 40 nm × 1.5 nm); a monatomic step is running vertically through the image with a lower terrace (dark) and an upper terrace (bright). The arrows mark positions 1 and 2 on the chains where *z-V* spectroscopy has been performed (see panel (b)). (b) *z-V* spectroscopy taken at different positions within the chains.

References:

[1] Cuniberti, G.; Fagas, G.; Richter, K. (eds.) Introducing Molecular Electronics. *Lecture Notes in Physics* **2005,** 680 (Springer, Berlin, Heidelberg 2005), DOI 10.1007/b101525

[2] Hang, Q.; Wang, F; Carpenter, P. D.; Zemlyanov, D; Zakharov, D.; Stach, E. A.; Buhro, W.E.; Janes, D. B. Role of Molecular Surface Passivation in Electrical Transport Properties of InAs Nanowires. *Nano Lett.* **2008**, *8*, 49-55

[3] Groll, J.; Möller, M. Star Polymer Surface Passivation for Single-Molecule Detection. *Methods Enzymol.* **2010**, *472, 1-18*

[4] Srivastava, G. P. Surface passivation by dissociative molecular adsorption. *Vacuum* **2002**, *67, 11-20*

[5] Schreiber, H. P. ; Wertheimer, M. R.; Wrobel, A. M. Corrosion protection by plasma-polymerized coatings. *Thin Solid Films* **1980**, *72*, 487-494

[6] Santos, J. R.; Mattoso, L. H. C.; Motheo, A. J. Investigation of corrosion protection of steel by polyaniline films. *Elechrochim. Acta* **1998**, *43*, 309-313

[7] Khramov, A. N.; Voevodin, N. N.; Balbyshev, V. N.; Donley, M. S. Layer-by-Layer Assembled Nanocontainers for Self-Healing Corrosion Protection. *Adv. Mater.* **2006**, *18*, 1672-1678

[8] Krishnan, R.S.; Mackay, M.E.; Hawker, C.J.; Van Horn, B. Influence of Molecular Architecture on the Dewetting of Thin Polystyrene Films. *Langmuir* **2005**, 21, 5770-5776

[9] Burke, S.A.; Topple, J.M.; Grütter, P. Molecular Dewetting on Insulators. *J. Phys. Cond. Matter.* **2009**, *21*, 423101

[10] Wang, A.; Essner, A.; Polineni, V.K.; Stark, C.; Dumbleton, J.H. Lubrication and wear of ultra-high molecular weight polyethylene in total joint replacements. *Tribol. Intern.* **1998**, *31*, 17

[11] Tsukruk, V. V. Molecular Lubricants and Glues for Micro- and Nanodevices. *Adv. Mater.* **2001**, *13*, 95-108

[12] Hsu, S.M. Molecular basis of lubrication. *Tribol. Intern.* **2004**, *37*, 553-559

[13] Sayari, A. Catalysis by Crystalline Mesoporous Molecular Sieves. *Chem. Mater.* **1996**, *8*, 1840-1852

[14] Noyori, R.; Ohkuma, T. Asymmetric Catalysis by Architectural and Functional Molecular Engineering: Practical Chemo- and Stereoselective Hydrogenation of Ketones. *Angew. Chem. Int. Ed.* **2001**, *40*, 40-73

[15] Heriot, S. Y.; Jones, R. A. L. An interfacial instability in a transient wetting layer leads to lateral phase separation in thin spin-cast polymer-blend films. *Nature Mat.* **2005**, *4*, 782-786

[16] Häkkinen, H. The gold-sulfur interface at the nanoscale. *Nature Chem.* **2012**, *4*, 443-455

[17] Cuevas, J. C.; Scheer, E. Molecular Electronics by World Scientific Series in Nanoscience and Nanotechnology. **2010**, Vol. 1, World Scientific Publishing Co. Pte. Ltd.

[18] Eberle, F.; Saitner, M.; Boyen, H.-G.; Kučera, J.; Groß,A.; Romanyuk, A.; Oelhafen, P.; D'Olieslaeger, M.; Manolova, M.; Kolb, D. M. A molecular "double decker" - extending the limits of current metal-molecule hybrid structures. *Angew. Chem., Int. Ed.* **2010**, *49*, 341-345

[19] Muglali, M. I.; Liu, J.; Bashir, A.; Borissov, D.; Xu, M.; Wang, Y.; Wöll, C.; Rohwerder, M. On the complexation kinetics for metallization of organic layers: palladium onto a pyridine-terminated araliphatic thiol film. *Phys. Chem. Chem. Phys.* **2012**, *14*, 4703-4712

[20] Muglali, M. I.; Bashir, A.; Birkner, A.; Rohwerder, M. J. Hydrogen as an optimum reducing agent for metallization of self-assembled monolayers. *Mater. Chem.* **2012**, *22*, 14337-14340

[21] Sawaguchi, T.; Mizutani, F.; Taniguchi, I. Direct Observation of 4-Mercaptopyridine and Bis(4-pyridyl) Disulfide Monolayers on Au(111) in Perchloric Acid Solution Using In Situ Scanning Tunneling Microscopy. *Langmuir* **1998**, *14*, 3565–3569

[22] Zhou, W.; Baunach, T.; Ivanova, V.; Kolb, D. M. Structure and Electrochemistry of 4,4'-Dithiodipyridine Self-Assembled Monolayers in Comparison with 4-Mercaptopyridine Self-Assembled Monolayers on Au(111). *Langmuir* **2004**, *20*, 4590-4595

[23] Ulusoy, I. S.; Scribano, Y.; Benoit, D. M.; Tschetschetkin, A.; Maurer, N.; Koslowski, B.; Ziemann, P. Vibrations of a Single Adsorbed Organic Molecule: Anharmonicity Matters! *Phys. Chem. Chem. Phys.* **2011**, *13*, 612-618

[24] Nuzzo, R. G.; Zegarski, B. R.; Dubois, L. H. Fundamental Studies oft he Chemisorption of Organosulfur Compounds on Au(111). Implications for Molecular Self-Assembly on Gold Surfaces. *J. Am. Chem. Soc.* **1987**, *109*, 733-740

[25] Grönbeck, H.; Curioni, A; Andreoni, W. Thiols and Disuflides on the Au(111) Surface: The Headgroup-Gold Interaction *J. Am. Chem. Soc.* **2000**, *122*, 3839-3842

[26] Lavrich, D. J.; Wetterer, S. M.; Beernasek, S. L.; Scoles, G. Physisorption and Chemisorption of Alkanethiols and Alkyl Sulfides on Au(111) *J. Phys. Chem. B* **1998**, *102*, 3456-3465

[27] De Renzi, V.; Rousseau, R.; Marchetto, D.; Biagi, R. Scandolo, S.; del Pennino, U. *Phys. Rev. Lett.* **2005**, *95*, 046804

[28] Maksymovych, P; Sorescu, D. C.; Yates J. T. Jr. Gold-Adatom-Mediated Bonding in Self-Assembled Short-Chain Alkanethiolate Species on the Au(111) Surface *Phys. Rev Lett.* **2006**, *97*, 146103

[29] Tkatchenko, A.; Romaner, L.; Hofmann, O.; Zojer, E.; Ambrosch-Draxl, C.; Scheffler, M. Van der Waals Interactions Between Organic Adsorbates and at Organic/Inorganic Interfaces. *MRS Bulletin* **2010**, *35*, 435-442

[30] Grimme, S.; Antony, J.; Ehrlich, S.; Krieg, H. A consistent and accurate ab initio parametrization of density functional dispersion correction (DFT-D) for the 94 elements H-Pu. *J. Chem. Phys.* **2010**, *132*, 154104

[31] Tkatchenko, A.; Scheffler, M. Accurate Molecular Van Der Waals Interactions from Ground-State Electron Density and Free-Atom Reference Data. *Phys. Rev. Lett.* **2009**, *102*, 073005

[32] Tonigold, K.; Groß, A. Adsorption of small aromatic molecules on the (111) surfaces of noble metals: A density functional theory study with semiempirical corrections for dispersion effects. *J. Chem. Phys.* **2010**, *132*, 224701

[33] McNellis, E. R.; Meyer, J.; Reuter, K. Azobenzene at coinage metal surfaces: Role of dispersive van der Waals interactions. *Phys. Rev. B* **2009**, *80*, 205414

[34] Koslowski, B.; Dietrich, Ch.; Tschetschetkin, A.; Ziemann, P. Design of an extremely stable low-temperature ultrahigh vacuum scanning tunneling microscope. *Rev. Sci. Instrum.* **2006**, *77*, 063707

[35] Kresse, G.; Furthmüller, J. Efficient iterative schemes for ab initio total-energy calculations using a plane-wave basis set. *Phys. Rev. B* **1996**, *54*, 11169-11186

[36] Blum, V.; Gehrke, R.; Hanke, F.; Havu, P.; Havu, V.; Ren, X.; Reuter, K.; Scheffler, M. Ab initio molecular simulations with numeric atom-centered orbitals. *Computer Physics Communications*, **2009**, *180*, 2175-2196

[37] Perdew, J. P.; Burke, K.; Ernzerhof, M. Generalized Gradient Approximation Made Simple. *Phys. Rev. Lett.* **1996**, *77*, 3865-3868

[38] Blöchl, P. E. Projector augmented-wave method. *Phys. Rev. B* **1994**, *50*, 17953-17979

[39] Kresse, G.; Joubert, D. From ultrasoft pseudopotentials to the projector augmented-wave method. *Phys. Rev. B* **1999**, *59*, 1758-1775

[40] Tersoff, J.; Hamann, D. R. Theory and Application for the Scanning Tunneling Microscope. *Phys. Rev. Lett.* **1983**, *50*, 1998-2001

[41] Kučera, J.; Groß, A. Adsorption of 4-mercaptopyridine on Au(111): a periodic DFT study. *Langmuir* **2008**, *24*, 13985-13992

[42] Pfeifer, H.; Koslowski, B.; Ziemann, P. Deconvolution of the density of states of tip and sample through constant-current tunneling spectroscopy. *Beilstein J. Nanotechnol*. **2011**, *2*, 607-617

[43] Ziegler, M.; Néel, N.; Sperl, A.; Kröger, J.; Berndt**,** R. Local density of states from constant-current tunneling spectra. *Phys. Rev.* B **2009**, *80*, 125402

[44] Koslowski, B.; Pfeifer, H.; Ziemann, P. Deconvolution of the electronic density of states of tip and sample from scanning tunneling spectroscopy data: Proof of principle. *Phys. Rev.* B **2009**, *80*, 165419

[45] Kliewer, J.; Berndt, R.; Chulkov, E. V.; Vilkin, V. M.; Echenique, P. M.; Campin, S. Dimensionality Effects in the Lifetime of Surface States. *Science* **2000**, *288*, 1399-1402

[46] Koslowski, B.; Dietrich, C.; Tschetschetkin, A.; Ziemann, P. Evaluation of scanning tunneling spectroscopy data: Approaching a quantitative determination of the electronic density of states. *Phys. Rev. B* **2007**, *75*, 035421

[47] Koslowski, B.; Tschetschetkin, A.; Maurer, N.; Ziemann, P. 4-Mercaptopyridine on Au(111): a scanning tunneling microscopy and spectroscopy study. *Phys. Chem. Chem. Phys.* **2011**, *13*, 4045-4050

[48] Koslowski, B.; Tschetschetkin, A.; Maurer, N.; Mena-Osteritz, E.; Bäuerle, P.; Ziemann, P. Terthiophene on Au(111): A scanning tunneling microscopy and spectroscopy study. *Beilstein J. Nanotechnol.* **2011**, *2*, 561-568

[49] Rasband, W.S. ImageJ, U. S. National Institutes of Health, Bethesda, Maryland, USA, http://imagej.nih.gov/ij/, 1997-2011

[50] bwGRiD, member of the German D-Grid initiative, funded by the Ministry of Education and Research (Bundesministerium für Bildung und Forschung) and the Ministry of Science, Research and the Arts Baden-Württemberg (Ministerium für Wissenschaft, Forschung und Kunst Baden-Württemberg), see http://www.bw-grid.de